International Journal of Solids and Structures 46 (2009) 2255–2264

Contents lists available at ScienceDirect

International Journal of Solids and Structures

journal homepage: www.elsevier.com/locate/ijsolstr

Mullins effect and cyclic stress softening of filled elastomers by internal sliding and friction thermodynamics model

S. Cantournet [a,*], R. Desmorat [b], J. Besson [a]

[a] MINES ParisTech, MAT-Centre des Matériaux, CNRS UMR 7633, BP 87, 91003 Evry Cedex, France
[b] LMT-Cachan (ENS Cachan/CNRS/Universite Paris 6/UniverSud Paris), 61 Av. du President Wilson, F-94230 Cachan, France

ARTICLE INFO

Article history:
Received 7 May 2008
Received in revised form 18 October 2008
Available online 29 January 2009

Keywords:
Elastomers
Hysteresis
Stress softening
Mullins effect
Nonlinear behavior

ABSTRACT

Elastomers are characterized by their ability to undergo large elastic deformation. Nevertheless, their behavior exhibits stress softening, hysteresis and cyclic softening. The first phenomenon, known as Mullins effect, is commonly assumed to be either the result of an evolution in the hard and soft domain microstructure whereby the effective volume fraction of the soft domain increases with stretch or the result of irreversible damage in the material or combination of both. Hysteresis and cyclic stress softening are often considered as the result of the effect of stress relaxation. Based on the physical structure of filled elastomers, the present study shows that the Mullins effect, hysteresis and cyclic softening can be modeled by dissipative friction phenomena due to internal sliding of the macromolecular chains and to sliding of the connecting chains on the reinforcing filler particles. This implies that the three effects are in fact related to one single deformation process. The proposed analysis allows to identify the state variables and to build a thermodynamic potential which accounts for the nonlinearity of the material behavior and for a time independent hysteresis. The constitutive model is 3D. Written in a rate form it applies to complex loadings: monotonic, cyclic, random fatigue, etc. Filled elastomers hysteresis loops and cyclic softening are represented with no need to introduce neither damage nor viscosity. The model was implemented in a Finite Element software to simulate a metal/elastomer lap joint. Good agreement with experiment was achieved.

1. Introduction

The rubber material has a singular mechanical behavior. It is a material which undergoes large strains (a few hundreds of percents) when loaded and exhibits a highly nonlinear behavior characterized by four main phenomena:

- at low strains it behaves as an linear elastic material whereas at large strain it exhibits a nonlinear elastic behavior,
- a rate-dependency,
- at large strains hysteresis loops appear when unloading,
- under cyclic loading conditions, filled elastomers present a loss of stiffness leading to cyclic stress softening and stress hysteresis.

The third phenomena is well known as the Mullins effect (Mullins, 1947). This mechanism of stress softening is characterized by a decrease of the stress on unloading compare to the stress on loading at the same strain. The most important assumption of Mullins model is that the reloading path is the same as the unloading path as long as the maximum strain of the first loading is not reached. Fig. 1 shows the behavior of an idealized material corresponding to Mullins effect only. But actual soft materials have a more complex inelastic behavior. In tests with constant displacement amplitude, the stress drop between successive loading cycles is especially important during the first and second cycles and becomes negligible after about 5–10 cycles. A stationary state with constant stress amplitude and stabilized hysteresis loop is then reached after several cycles (see Fig. 2).

The Mullins effect is the most studied phenomenon in filled elastomers. At present, Mullins effect description is based on two main approaches. The first one was initially proposed by Mullins (Mullins and Tobin, 1965; Mullins and Tobin, 1954); it is based on a two-phase mechanical model: the material is assumed to contain both soft and hard rubber phases. Under loading, the hard rubber phase is transformed into soft rubber. Harwood and Payne (1966, 1968) introduced an evolution law for the soft phase volume fraction and accounted for the strain amplification in the soft phase induced by the hard phase considered as rigid. Miehe (1995) and Qi and Boyce (2004) generalized this approach and implemented strain amplification functions within constitutive models for Finite Element (FE) applications.

* Corresponding author. Tel.: +33 160 76 30 52; fax: +33 160 76 31 50.
E-mail address: sabine.cantournet@ensmp.fr (S. Cantournet).

0020-7683/$ - see front matter © 2009 Elsevier Ltd. All rights reserved.
doi:10.1016/j.ijsolstr.2008.12.025

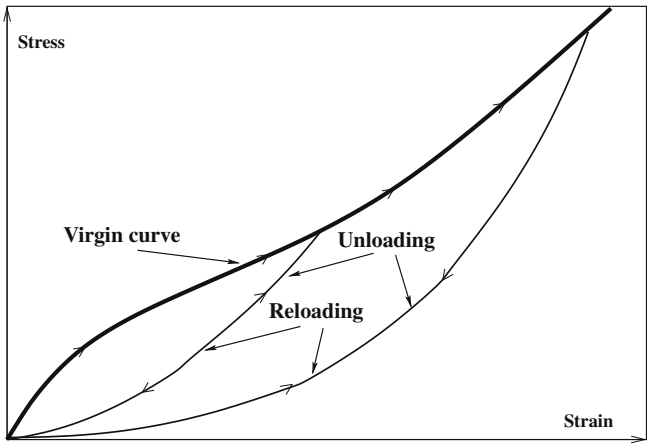

Fig. 1. Idealized Mullins mechanical behavior.

The second approach is based on the thermodynamics framework of Continuum Damage Mechanics (Simo, 1987; Miehe and Keck, 2000). This approach implicitly implies that damage corresponds to breaking of weak polymers chains as explained by Bueche (1960). It introduces fairly complex large strain constitutive equations coupled with damage able to model Mullins effect. Most recent models for rubber depend on the maximum stretch history (Ogden and roxburgh, 1999; Miehe, 1995; Andrieux et al., 1997). Simo's model was improved by use of microscopic considerations (Godvindjee and Simo, 1991). Johnson and Beatty (1993) and Beatty and Krishnaswamy (2000) adopted a much simpler approach based on an original two phase analysis (Mullins and Tobin, 1965). This uniaxial model was extended to 3D cases (Zuniga and Beatty, 2002) by introducing a damage function depending on the maximum elongation over a loading cycle. These approaches are useful when cycles are clearly defined but prove limited for complex loadings such as random fatigue.

The purpose of this study is propose a new model for Mullins effect, cyclic stress softening and hysteresis loop assuming that these three mechanisms are related to internal friction and sliding of molecular chains. First (Section 2) the foundations of the model are presented based on a description of the physical structure of elastomers to explain their deformation processes. This description is used to build the new model with a restricted number of parameters, to define the relevant thermodynamics variables and their evolution laws and to fit the associated material parameters. From this analysis one then establishes a 3D thermodynamics model with internal variables written in a rate form allowing for the representation of hysteresis loops and stress softening of elastomers (Section 3). The numerical implementation of the model is presented in Section 4 together with two possibilities to account for incompressibility. The model is fitted for one natural rubber and for a synthetic rubber both containing filler particles (Section 5). Examples of application are given in Section 6.

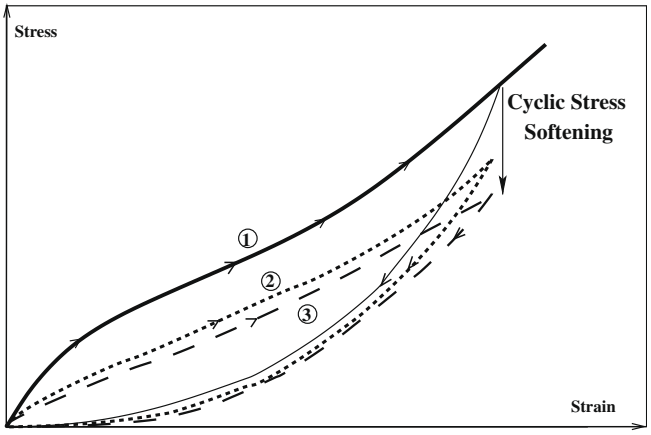

Fig. 2. Actual mechanical behavior of elastomer.

2. Mechanisms of filler/chain slip in elastomers

Elastomers are amorphous polymers made up of long flexible macromolecular chains folded up on themselves. This flexibility is due to freely rotating links permitted by the weak secondary forces between the molecules (chemical interactions between macromolecular chains). The chains can slip over one another under loading because the mechanical energy exceeds very quickly the energy of the secondary forces such as van der Waals forces. Thus, from a micromechanical point of view one can regard this material as a viscous liquid. Vulcanization creates bridges between the chains and produces a three-dimensional network. Due to these links, viscous flow is inhibited so that an elastic solid behavior prevails. Before vulcanization, the addition of particles (carbon black, silica) to rubber leads to significant improvements of the physical and the mechanical properties of the material. These additions of filler also contribute to an increase of the strain hysteresis under cyclic loading (Vidal and Donnet, 1986): the macromolecular chains are slipping and sliding with friction over one another (Bueche, 1960); the chains connected to the reinforcing filler are slipping and sliding with friction on these particles (see Fig. 3). The macromolecular chains connected to the surfaces of filler particles undergo a deformation state close to the macroscopic deformation state (Dannenberg, 1975). As deformation increases, the shortest chains undergo a stress concentration and slip on the filler surfaces. Consequently, in order to model the mechanical hysteresis loops of filled rubber it is necessary to introduce thermodynamics internal variables. In the following one introduces as variable in the constitutive model an average measure of the internal slips (denoted next α in 1D or $\boldsymbol{\alpha}$ in 3D) and its associated variable (X or $\boldsymbol{X}$) which will represent the residual micro-stresses.

By performing relaxations during a loading-unloading tensile test the existence of a residual non-viscous hysteresis is exhibited as shown in Fig. 4 (with F the load, S_0 the initial cross-section, λ the engineering strain or elongation). The test is performed as follows. A displacement U is applied first up to a given value (corresponding elongation λ_A) and to the corresponding force F_A (point A, later: points B, C, D, E). The displacement is then kept constant during 24 h and stress relaxation is observed (at given elongation $\lambda = \lambda_A$). The displacement is then increased up to a displacement U_B (corresponding to λ_B) with again a relaxation stage, and so on for points C, D, E. During unloading, the same procedure is followed with relaxations performed at the same given displacements U_D, U_C, U_B, U_A than for the previous loading. At the end of each relaxation stage, the material almost is completely relaxed. A virtual

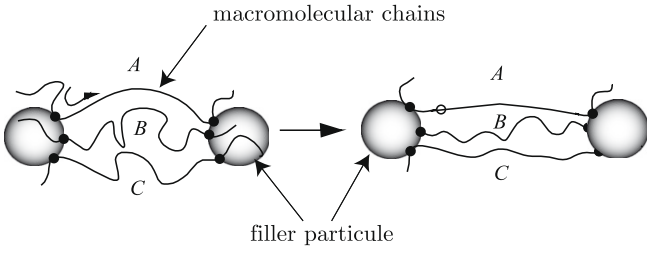

Fig. 3. Chains and filler interaction (Dannenberg, 1975).

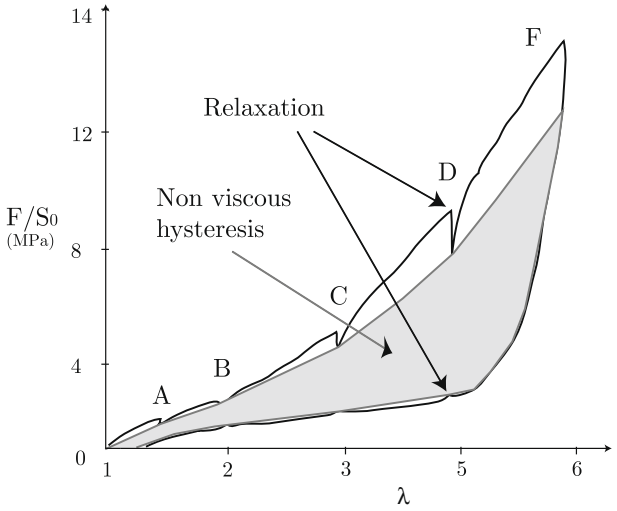

Fig. 4. Non-viscous residual hysteresis – experiment on filled NR (black line).

response with no time dependence can then be drawn (grey area of Fig. 4). Consequently, the response of this test exhibits a non-viscous time or rate independent hysteresis. Note that stress relaxation corresponding to unloading is much reduced compared to loading. Note also that permanent strains encountered here are small and will be neglected in further modeling. According to these observations, viscosity will also be neglected as it is not the primary cause of hysteresis and stress softening. For practical applications, the model build next will then apply to the study of the short term behavior of materials and structures submitted to slow loading.

The model does not include damage to represent softening which is induced in the model by nonlinear kinematic hardening as it is commonly done in the case of metals (Lemaitre and Chaboche, 1985). Note that actual damage (i.e. nucleation and growth of voids and microcracks) is expected to grow very slowly during the very first cycles and to gradually increase as the number of cycles increases up to rupture (Lemaitre and Desmorat, 2005).

3. Finite strain model for internal sliding and friction (ISF model)

3.1. Thermodynamics potential and state laws

The previous study of the micro-structure of elastomer materials coupled with the physical understanding of Mullins effect enables to highlight the existence of a time independent hysteresis and then of a non-viscous internal friction. Several studies have already proposed to model hysteresis without viscosity but with the assumption of a state of small deformations: see for instance the work of Burr et al. (1997) for composite materials and of Dragon and Halm (1998) for concrete. Following these authors, the 1D expressions for the thermodynamics potential for the different models can be written in the synthetic general form:

$$\rho\psi = a\,\varepsilon^2 + b\,(\varepsilon - \epsilon^\pi)^2 + c\,\alpha^2 \tag{1}$$

where $\rho\psi$ is the free energy density, ρ the density, ε the strain, and where α and ϵ^π represent the internal sliding and inelastic deformation of the material due to friction and where the coefficients a, b, c may depend on internal variables such as damage.

To model hysteresis and non-viscous internal friction in the framework of finite strains, the same separation of the free energy into three terms is kept:

- an energy W_1 of a hyperelastic type, function of transformation gradient $\boldsymbol{F}$,
- an energy W_2 of a hyperelastic type with inelastic deformation $\boldsymbol{E}^\pi$,
- an energy stored into the material, due to friction and function of the internal slip variable $\boldsymbol{\alpha}$, a second order tensor.

For simplicity, the thermodynamics potential is written in its Lagrange form (in the reference configuration) as a function of the Green–Lagrange strain tensor $\boldsymbol{E}$ (associated with the second Piola–Kirchhoff stress tensor $\boldsymbol{S}$),

$$\rho_0\psi = W_1(\boldsymbol{E}) + W_2(\boldsymbol{E} - \boldsymbol{E}^\pi) + \frac{1}{2}C_x\,\boldsymbol{\alpha} : \boldsymbol{\alpha} \tag{2}$$

where ρ_0 is the density of the undeformed material, C_x is a material parameter and where the state variables are the couples $(\boldsymbol{S},\boldsymbol{E})$, $(-\boldsymbol{S}_2,\boldsymbol{E}^\pi)$ and $(\boldsymbol{X},\boldsymbol{\alpha})$. The internal variable $\boldsymbol{\alpha}$, represents both solid friction between the long macromolecular chains and friction between the macromolecular chains and the filler reinforcing particles leading to Mullins effect. The term $\frac{1}{2}C_x\,\boldsymbol{\alpha} : \boldsymbol{\alpha}$ is the stored energy density due to residual micro-stresses. Note that the model could be easily extended by introducing several internal slip variables (i.e. $(\boldsymbol{\alpha}_i,\boldsymbol{X}_i)$ with $i = 1,\ldots,N$) which could be interpreted as corresponding to different sliding mechanisms.

The state laws classically derive from the thermodynamics potential (Truesdell and Noll, 1965). The constitutive equations obtained are:

$$\begin{aligned}
\boldsymbol{S} &= \frac{\partial W_1}{\partial \boldsymbol{E}} + \frac{\partial W_2}{\partial \boldsymbol{E}} \\
\boldsymbol{S}_2 &= -\frac{\partial W_2}{\partial \boldsymbol{E}^\pi} = \frac{\partial W_2}{\partial \boldsymbol{E}} \\
\boldsymbol{X} &= \rho_0\frac{\partial \psi}{\partial \boldsymbol{\alpha}} = C_x\,\boldsymbol{\alpha}
\end{aligned} \tag{3}$$

so that the second Piola–Kirchhoff stress tensor is made up of two parts $\boldsymbol{S}_1 = \partial W_1/\partial \boldsymbol{E}$ and $\boldsymbol{S}_2 = \partial W_2/\partial \boldsymbol{E}$. Eq. (3) define the variables associated with $\boldsymbol{E}^\pi$ and $\boldsymbol{\alpha}$, the variable $\boldsymbol{X}$ being the residual micro-stress due to internal friction.

The expressions for the potentials W_1 and W_2 are chosen according to existing hyperelastic densities such as Mooney's, Hart-Smith's or others (Rivlin, 1948; Arruda and Boyce, 1993; Lambert-Diani and Rey, 1999)

$$W_1 = m_1\,(I_1 - 3) + m_2\,(I_2 - 3) \quad \text{Mooney} \tag{4}$$

$$W_1 = h_1 \int \exp(h_3(I_1 - 3)^2)\,dI_1 + 3h_2 \ln\left(\frac{I_2}{3}\right) \quad \text{Hart-Smith} \tag{5}$$

where I_1, I_2 are the invariants of the right Cauchy–Green tensor $\boldsymbol{C} = \boldsymbol{F}^T \cdot \boldsymbol{F}$ ($\boldsymbol{F}$ is the transformation gradient)

$$\begin{aligned}
I_1 &= tr\,\boldsymbol{C} \\
I_2 &= \frac{1}{2}\left[(\mathrm{tr}\boldsymbol{C})^2 - \mathrm{tr}\boldsymbol{C}^2\right] \\
I_3 &= J^2 = \det \boldsymbol{C}
\end{aligned} \tag{6}$$

where I_3 is the third invariant and represents the volume change. For the sake of simplicity the energy density W_2 is expressed as a quadratic function of the first invariant I_1 and of the trace of $\boldsymbol{E}^\pi$, introducing one material parameter only (C_{20}),

$$W_2 = 4\,C_{20}(\mathrm{tr}(\boldsymbol{E} - \boldsymbol{E}^\pi))^2 = C_{20}\,(I_1 - 2\mathrm{tr}\,\boldsymbol{E}^\pi - 3)^2 \tag{7}$$

so that

$$\boldsymbol{S_2} = \frac{\partial W_2}{\partial \boldsymbol{E}} = 8\,C_{20}(\mathrm{tr}(\boldsymbol{E} - \boldsymbol{E}^\pi))\boldsymbol{1} \tag{8}$$

This choice is consistent with the fact, at least moderate strain levels, the I_2-terms do not have a major effect on the monotonic response of rubber-like materials (Lambert-Diani and Rey, 1999). Such terms are nevertheless already taken into account within W_1. Indeed, another form for W_2 could be used without any restriction. Expressing W_2 as a function of the trace of $\boldsymbol{E}-\boldsymbol{E}^{\pi}$ implies that $\boldsymbol{S}_2$ is spherical which is not the case if W_2 depends on $I_2(\boldsymbol{E}-\boldsymbol{E}^{\pi})$.

3.2. Evolution laws for internal friction

The evolution laws are derived here from a criterion function f analogous to the yield surface in plasticity:

$$\begin{aligned} &f<0 \text{ or } \dot{f}\neq 0 \quad \text{no internal friction} \\ &f=0 \text{ and } \dot{f}=0 \quad \text{internal friction occurs} \end{aligned} \tag{9}$$

The chosen sliding criterion is function of the stress $\boldsymbol{S}_2$ and of the residual micro-stress $\boldsymbol{X}$:

$$f=\|\boldsymbol{S}_2-\boldsymbol{X}\|-\sigma_s \tag{10}$$

where σ_s is the sliding threshold of friction (irreversibility threshold). The norm $\|\cdot\|$ is such that $\|\boldsymbol{A}\|=\sqrt{\boldsymbol{A}:\boldsymbol{A}}$.

The proposed model is non-associated as the normality rule leading to the evolutions laws is not written on the criterion function f but on the dissipation potential F defined by:

$$F=f+\frac{\gamma}{2C_x}\boldsymbol{X}:\boldsymbol{X} \tag{11}$$

with C_x (already introduced) and γ are material parameters accounting for nonlinear sliding. The second term of Eq. (11) is chosen similar to the term introduced in metals plasticity to model nonlinear kinematic hardening. Considered here for elastomers, it will lead to cyclic softening and, in addition, model Mullins effect which, as far as the model is concerned, corresponds to softening for the first cycle. Using linear kinematic hardening (i.e. $\gamma=0$), one gets a description of Mullins effect without further cyclic softening.

A Lagrange friction multiplier $\dot{\mu}$ (which is non-negative) is then introduced as for the generalized standard materials (Halphen, 1975). The evolution laws derive from the normality rule:

$$\dot{\mathscr{V}}_k=-\dot{\mu}\frac{\partial F}{\partial \mathscr{A}_k} \tag{12}$$

with the sets $\mathscr{V}=\{\boldsymbol{E}^{\pi},\boldsymbol{\alpha}\}$ (respectively $\mathscr{A}=\{-\boldsymbol{S}_2,\boldsymbol{X}\}$) of thermodynamics internal (respectively associated) variables. The evolution laws are then expressed as:

$$\dot{\boldsymbol{E}}^{\pi}=\dot{\mu}\frac{\boldsymbol{S}_2-\boldsymbol{X}}{\|\boldsymbol{S}_2-\boldsymbol{X}\|}=\dot{\mu}\boldsymbol{n} \tag{13}$$

$$\dot{\boldsymbol{\alpha}}=\dot{\boldsymbol{E}}^{\pi}-\frac{\gamma}{C_x}\boldsymbol{X}\,\dot{\mu} \tag{14}$$

From the first relation, one gets $\dot{\mu}=\|\dot{\boldsymbol{E}}^{\pi}\|$ and define

$$\pi=\int\left\|\dot{\boldsymbol{E}}^{\pi}\right\|dt \tag{15}$$

as a cumulative measure of the internal sliding. Moreover from the evolution law (14) for the internal slip $\boldsymbol{\alpha}$ considered altogether with the state law (3), the evolution law for the residual micro-stress $\boldsymbol{X}$ reads (provided C_x is a constant):

$$\dot{\boldsymbol{X}}=C_x\dot{\boldsymbol{E}}^{\pi}-\gamma\boldsymbol{X}\,\dot{\pi} \tag{16}$$

and is similar to Armstrong–Frederick (1966) law for the back stress in standard plasticity.

The friction multiplier $\dot{\mu}$ is finally calculated by means of the consistency condition $f=0$ and $\dot{f}=0$,

$$\dot{\mu}=\frac{\boldsymbol{n}:\dot{\boldsymbol{S}}_2}{h},\quad h=C_x-\gamma\boldsymbol{n}:\boldsymbol{X} \tag{17}$$

Note that a model describing viscosity could easily be obtained using a constitutive relation between $\dot{\mu}$ and f considered as an overstress. Such a relation may be $\dot{\mu}=\langle f/\kappa\rangle^n$ (Norton law) where κ and n are two additional material parameters. This description will allow representing the different stress relaxation behaviors observed during loading and unloading (see Fig. 4).

3.3. Positivity of the intrinsic dissipation

It can be easily checked that the intrinsic dissipation $\mathscr{D}=\boldsymbol{S}:\dot{\boldsymbol{E}}-\rho_0\dot{\psi}$ calculated by means of Clausius–Duhem inequality always remains positive. One has

$$\mathscr{D}=-\rho_0\frac{\partial\psi}{\partial\boldsymbol{E}^{\pi}}:\dot{\boldsymbol{E}}^{\pi}-\rho_0\frac{\partial\psi}{\partial\boldsymbol{\alpha}}:\dot{\boldsymbol{\alpha}}=\boldsymbol{S}_2:\dot{\boldsymbol{E}}^{\pi}-\boldsymbol{X}:\dot{\boldsymbol{\alpha}} \tag{18}$$

The state laws and the evolution laws allow to write the dissipation in the following form:

$$\mathscr{D}=\left(\sigma_s+\frac{\gamma}{C_x}\boldsymbol{X}:\boldsymbol{X}\right)\left\|\dot{\boldsymbol{E}}^{\pi}\right\|\geqslant 0 \tag{19}$$

and to conclude that $\mathscr{D}$ is positive for any 3D loading, including non-proportional loading, cyclic loading and random fatigue.

3.4. Tangent operator

A rate form for the proposed model can be derived, written as $\dot{\boldsymbol{S}}=\underline{\boldsymbol{L}}:\dot{\boldsymbol{E}}$, introducing the tangent operator $\underline{\boldsymbol{L}}$ (a fourth order tensor) composed of two parts: a hyperelastic part $\underline{\boldsymbol{L}}_{\text{hyper}}=\partial^2W_1/\partial\boldsymbol{E}^2$, known for existing hyperelastic energy densities, and a second part $\underline{\boldsymbol{L}}_2=\partial^2W_2/\partial\boldsymbol{E}^2$ combining the effects of the internal variables,

$$\begin{aligned} &\underline{\boldsymbol{L}}=\underline{\boldsymbol{L}}_{\text{hyper}}+\underline{\boldsymbol{L}}_2 \\ &\underline{\boldsymbol{L}}_2=8C_{20}\left(1-\frac{8C_{20}(\text{tr}(\boldsymbol{n}))^2}{h+8C_{20}(\text{tr}(\boldsymbol{n}))^2}\right)\boldsymbol{1}\otimes\boldsymbol{1} \end{aligned} \tag{20}$$

which are symmetric tensors even if the model is non-associated (i.e. when $F\neq f$ due to $\gamma\neq 0$) because W_2 depends only on the first invariant of $\boldsymbol{E}-\boldsymbol{E}^{\pi}$. $\underline{\boldsymbol{L}}_{\text{hyper}}$ for the different models is given by Holzapfel (2001).

4. Numerical implementation of the model

4.1. Implicit integration of constitutive equations

The constitutive equations classically consist of a set of differential equations expressed as evolution laws of the internal variables $\boldsymbol{E}^{\pi}$, $\boldsymbol{\alpha}$, and of the friction multiplier $\dot{\mu}$. These equations must be integrated over a finite time step expressed as $[t^0,t^1]$ so that the time increment is $\Delta t=t^1-t^0$. All the variables are assumed known at the beginning of the increment (i.e. at time t^0). The constitutive equations are assumed to be implemented in a standard displacement based Finite Element code, in which case the increment of the Green–Lagrange strain tensor, $\Delta\boldsymbol{E}$, is known over the time increment Δt as its rate of variation, $\underline{\dot{\boldsymbol{E}}}=\Delta\boldsymbol{E}/\Delta t$. The differential equations of the model are:

$$\begin{aligned} &\dot{\boldsymbol{E}}^{\pi}=\dot{\mu}\,\boldsymbol{n} \\ &\dot{\boldsymbol{\alpha}}=\dot{\boldsymbol{E}}^{\pi}-\gamma\dot{\mu}\,\boldsymbol{\alpha} \\ &\dot{\mu}=\frac{8C_{20}\text{tr}(\boldsymbol{n})\text{tr}\left(\underline{\dot{\boldsymbol{E}}}\right)}{8C_{20}\text{tr}(\boldsymbol{n})^2+C_x-\gamma\,\boldsymbol{n}:\boldsymbol{X}} \end{aligned} \tag{21}$$

where $\dot{\mu}$ is obtained by use of the consistency condition $\dot{f}=0, f=0$. The previous set of constitutive equations can be integrated using a time adaptative explicit integration method such as the Runge–Kutta method. However, significantly improved computation times are obtained using an implicit mid-point integration method (Simo et al., 1985). In this case, Eq. (21) is replaced by:

$$\begin{aligned}&\Delta \boldsymbol{E}^{\pi}=\Delta\mu\,\boldsymbol{n}^{\theta}\\&\Delta\boldsymbol{\alpha}=\Delta\boldsymbol{E}^{\pi}-\gamma\Delta\mu\,\boldsymbol{\alpha}^{\theta}\\&f^{\theta}=\|\boldsymbol{S}_2^{\theta}-\boldsymbol{X}^{\theta}\|-\sigma_s=0 \text{ or better } f^{1}=\|\boldsymbol{S}_2^{1}-\boldsymbol{X}^{1}\|-\sigma_s=0\end{aligned}\tag{22}$$

where $(\Delta\boldsymbol{E}^{\pi},\Delta\boldsymbol{\alpha},\Delta\mu)$ represent the finite increments of the internal variables over the time increment Δt. The parameter $\theta\in[0,1]$ allows a fully implicit $(\theta=1)$ or a semi-implicit $(0<\theta<1)$ integration scheme. Details of the implementation can be found in Appendix A.

4.2. Numerical formulations to enforce incompressibility

The model, as implemented in the previous section, can be used as a user defined material behavior in a standard displacement based large strain FE code. However, elastomers are usually nearly incompressible so that special treatments are usually required to properly carry out simulations (Ogden, 1982).

In this work two finite element approaches are used. The first one relies on a standard displacement-based formulation whereas the second one uses a mixed displacement–pressure formulation. In the first case, incompressibility is obtained enforced by introducing a large bulk modulus (Oden, 1972). This method exhibits locking when resistance to volume deformation associated to the penalty term $\frac{1}{2}Kp_0U(I_3)$ is much higher compared to the resistance to isochoric deformation. $U(I_3-1)$ is chosen as a quadratic form which respects energy and strain properties defined by Doll and Schweizerhof (2000). Using this method, strict incompressibility cannot be reached. The elementary stiffness matrix is ill-conditioned for large values of K. Selective-reduced integration method can be used to avoid pressure variations inside the elements (Hughes, 1980).

To eliminate the locking phenomena inherent to the displacement-based formulation, a mixed displacement–pressure formulation can be used (Simo et al., 1985; Taylor, 2000). The pressure field p is introduced as a Lagrange multiplier to enforce the incompressibility constraint $(J=\sqrt{I_3}=1)$. With such a mixed formulation, the modified invariants method deriving from Flory (1961) and Penn (1970) works is used. Note that the total second Piola–Kirchhoff stress $\boldsymbol{S}=\partial W_1/\partial\boldsymbol{E}+\partial W_2/\partial\boldsymbol{E}$ with this modified invariants is not only composed of the contribution S_1 and the contribution S_2. The total Piola–Kirchhoff stress transforms into the following expression:

$$\boldsymbol{S}=\bar{\boldsymbol{S}}_1+I_3^{-\frac{1}{3}}\bar{\boldsymbol{S}}_2-\frac{4}{3}C_{20}I_3^{-\frac{4}{3}}\left(\boldsymbol{C}^{-1}\otimes\boldsymbol{C}\right):\left(\bar{I}_1\mathbf{1}-\bar{\boldsymbol{C}}\right)\tag{23}$$

The $\bar{\boldsymbol{S}}_1$ is the isochoric hyperelastic part (Holzapfel, 2001) and Eqs. (7) and (8) can then be written using Penn invariants to define $\bar{\boldsymbol{S}}_2$. The corresponding tangent operator is given as:

$$\underline{\boldsymbol{L}}=\underline{\boldsymbol{L}}^{\text{iso}}_{\text{hyper}}-\underline{\boldsymbol{L}}_2I_3^{-\frac{1}{3}}+\left(\frac{8C_{20}(\text{tr}(\boldsymbol{n}:\underline{\boldsymbol{L}}_2))^2}{h+8C_{20}(\text{tr}(\boldsymbol{n}))^2}\right)\mathbf{1}\otimes\boldsymbol{n}-\left(\frac{1}{3}I_3^{-\frac{4}{3}}\right)\boldsymbol{S}_2\otimes\frac{\partial I_3}{\partial\boldsymbol{C}}\tag{24}$$

with $\underline{\boldsymbol{L}}_2$ given by Eq. (20) and $\underline{\boldsymbol{L}}^{\text{iso}}_{\text{hyper}}$ is the isochoric hyperelastic part (Holzapfel, 2001).

The mixed formulation associated with the modified invariant method proves more stable for multiaxial problem because in such cases the strain energy only depends on isochoric deformation. This point will be illustrated on lap joint computations in Section 6.

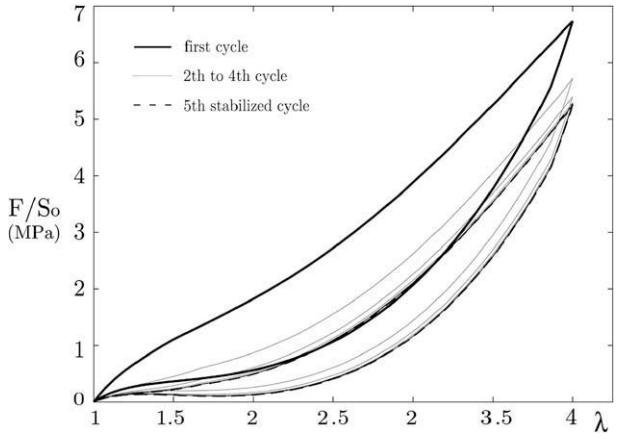

Fig. 5. Example of uniaxial cyclic response (nominal stress vs. elongation).

5. Hysteretic uniaxial response of the model

The simulation shown in Fig. 5 shows the ability of the new model to represent both the hysteresis and the cyclic softening. Material parameters are given in Table 1. They are chosen as realistic values for quasi-incompressible hyperelastic Mooney strain energy density for filled rubber. These parameters are used in the following parametric study. This parametric study can be used to define guidelines for parameter identification.

5.1. Parametric study and identification of the material parameters

The main features of the model can be highlighted by a parametric study of the hysteresis and of cyclic stress softening. Two groups of material parameters are identified. First, the parameters which are necessary to describe the hysteresis loop under the first loading–unloading path (C_{20} and σ_s). The second group includes the material parameters governing cyclic stress softening until stabilization (C_x and γ). The material parameters will be estimated using uniaxial tensile tests only.

5.1.1. Role of C_{20} and σ_s

The first loop of hysteresis is plotted in Fig. 6 in which the four stages of the model response are reported: (i) hyperelastic loading without sliding, (ii) dissipative loading with internal sliding and friction, (iii) hyperelastic unloading parametrized by its size ΔS_{11} and its slope $S_U=\partial S_{11}/\partial E_{11}$ at the point of initial unloading, and (iv) dissipative unloading with internal sliding and friction. S_{11} (respectively E_{11}) is component of the second Piola–Kirchhoff stress tensor (respectively Green–Lagrange strain tensor) in the loading direction. No permanent strains are obtained due to the spherical form of $\boldsymbol{S}_2$ stress tensor. The following remarks can be used as guidelines for the estimation of the first material parameters group:

- Parameter C_{20} strongly influences the slope S_U and slightly the linear unloading length ΔS_{11}. Fig. 7 shows the normalized slope S_U as a function of the maximum Green–Lagrange strain for dif-

Table 1
Materials parameters for the parametric study.

Hyperelasticity			Internal sliding			
m_1	m_2	K	C_{20}	C_x	σ_s	γ
1.85 MPa	0.26 MPa	500	1 MPa	10 MPa	1 MPa	5

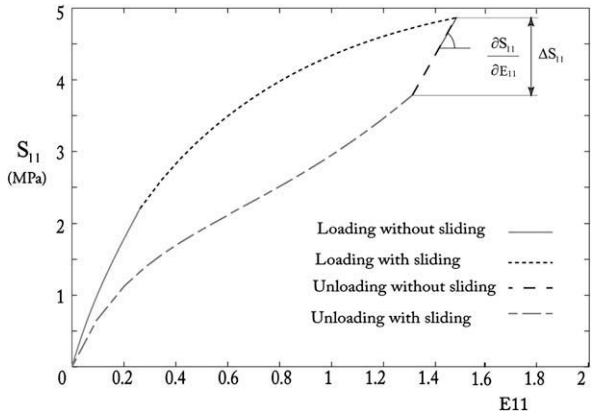

Fig. 6. First hysteresis loop indicated where sliding is acting ($\partial S_{11}/\partial E_{11} = S_U$).

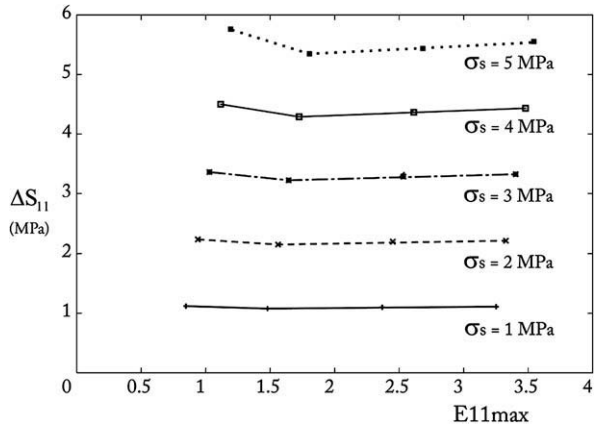

Fig. 8. Size of the hyperelastic unloading (ΔS_{11}) as a function of the maximum Green–Lagrange strain for different values of σ_s.

ferent values of C_{20}. The normalized value S_U/C_{20} only slightly depends on C_{20} so that S_U is almost a linear function of C_{20} for a fixed value of the strain.

- The area of the hysteresis loop essentially depends on the length ΔS_{11} of the unloading part without friction and of the slope S_U (Fig. 6).
- The irreversibility threshold σ_s influences strongly the length of the unloading without friction ΔS_{11} and very little its slope S_U. The influence of σ_s on S_U due to nonlinear elasticity. Fig. 8 illustrates the variation of the ΔS_{11} as a function of the Green–Lagrange strain for different values of σ_s. The normalized value $\Delta S_{11}/\sigma_s$ is almost independent on σ_s. It will depend on the chosen hyperelastic behavior.

5.1.2. Role of C_x and γ

Cyclic stress softening can be characterized by the amplitude of maximum stress decrease and by the number of cycles needed to reach a stabilized state. The effect of C_x and γ on softening is illustrated in Fig. 9 where $(S_{max})_1$ (respectively $(S_{max})_i$) is the maximum stress at cycle 1 (respectively i).

- Stress softening intensity depends on the ratio C_x/γ which is the saturation value of the residual micro-stress $\boldsymbol{X}$ in tensile loading. The amplitude of stress softening increases with increasing C_x/γ ratio. For a given ratio, softening is increased for high values of C_x and γ. Note that S_{max} increases with increasing C_x/γ.

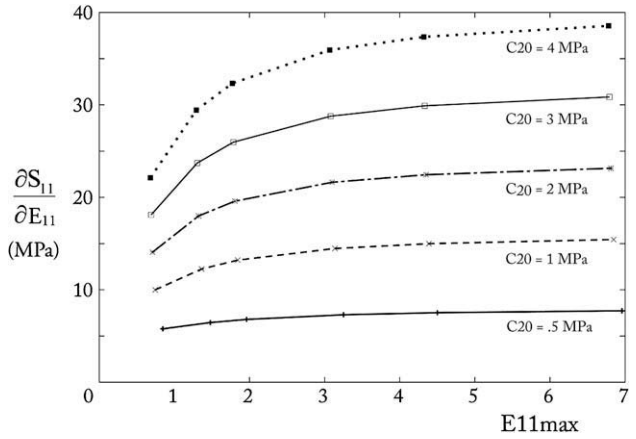

Fig. 7. Unloading stiffness ($S_U = \partial S_{11}/\partial E_{11}$) as a function of the maximum Green–Lagrange strain.

- The rate of stress softening for a given C_x/γ ratio increases with increasing C_x and γ.
- The effects of γ and C_x are strongly coupled.

5.1.3. Identification strategy

As a conclusion of this sensitivity analysis, parameters σ_s and C_{20} will be identified on the stage of hyperelastic unloading. Parameters C_x and γ will be identified on cyclic softening. In absence of stress softening (or if the stabilized cycle only is to be represented) $\gamma = 0$ will be used.

5.2. Stress–strain response of filled NR and filled SBR

The model was identified on a filled natural rubber (NR) and a filled styrene butadiene rubber (SBR). Experimental procedures are given in Cantournet (2002), Lapra (1999). Two loading paths were applied: (case (a)) two cycles with a maximum elongation $\lambda = 4$, (case (b)) two cycles with a maximum elongation $\lambda = 3$ followed by a cycle with a maximum elongation $\lambda = 4$. The identification of both materials was performed on loading case (a) and was validated on loading case (b). Figs. 10–12 show the response of the model for cyclic uniaxial loading for a filled SBR and a filled NR. The material parameters for the filled SBR were first identified using a Mooney hyperelastic law (see Table 3). As expected with this model, the sharp upturn at large strains is not represented. The parameters were then identified using a Hart-Smith hyperelastic law (see Table 4) which enables a much better modeling of the upturn (note that the Arruda and Boyce (1993) model could have been used for the same purpose). Both the shape and the size of the hysteresis loops are better modeled. The material parameters for the filled NR were identified using a Mooney hyperelastic law which proved sufficient in that case (parameters are given in Table 2). For both materials, the model response for the validation loading (case (b)) compares well with the experimental results. According to the remarks made in the previous section, the C_x/γ ratio for filled NR is larger than for filled SBR as cyclic stress softening is more pronounced for the filled NR.

6. Cyclic response of a metal/elastomer lap joint

The model was applied to simulate a cyclic shear experiment carried out for a metal/elastomer double lap-joint shown in Fig. 13. In such a test, deformation is non-uniform. Experiments were performed at the Paulstra–Hutchinson company using the previously mentioned filled NR. Dimensions of the specimens (in

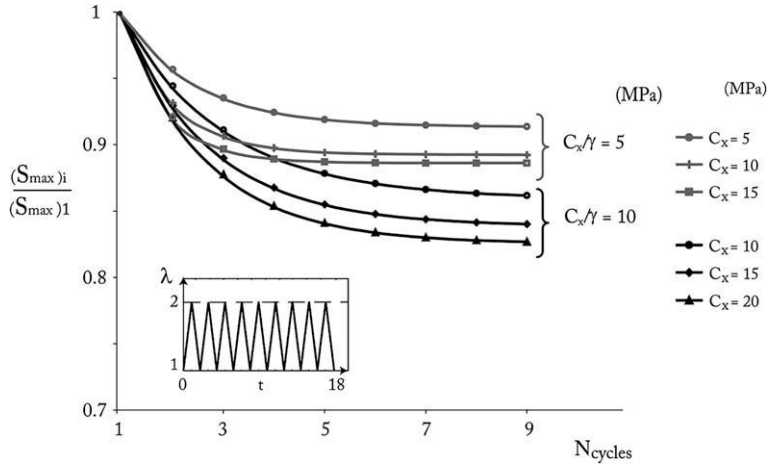

Fig. 9. Influence the ratio C_x/γ on stress softening for different values of C_x (MPa): cyclic softening as a function of the number of cycles (cycles are shown on the small graph).

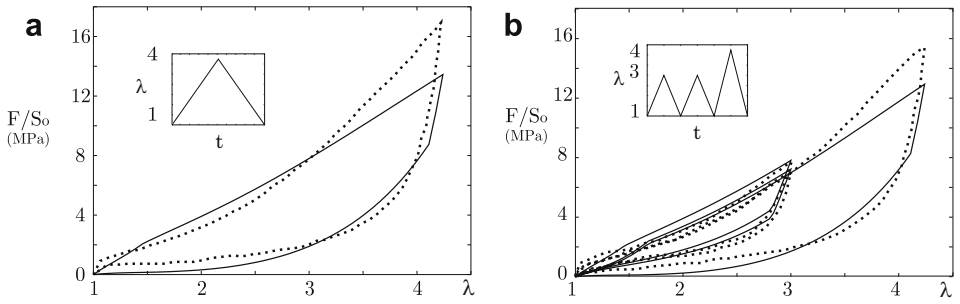

Fig. 10. Cyclic tension test: identification of SBR material parameters with Mooney hyperelastic law (experiment shown with a dashed line, the model with a solid line).

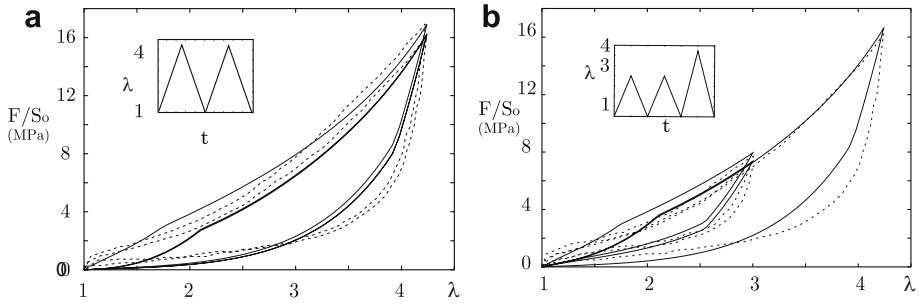

Fig. 11. Cyclic tension test: identification of SBR material parameters with Hart-Smith hyperelastic law (experiment shown with a dashed line, the model with a solid line).

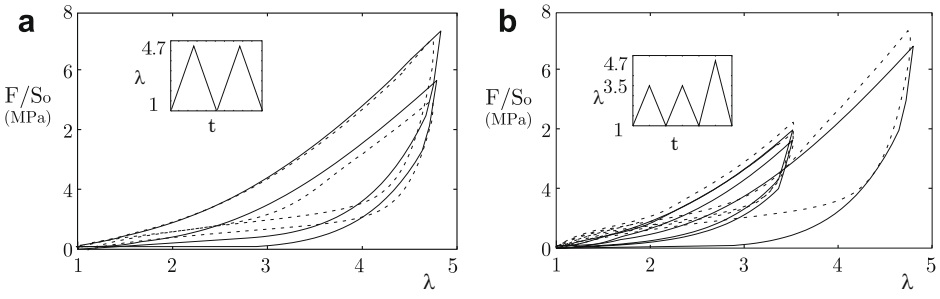

Fig. 12. Cyclic tension test: identification of NR material parameters with Mooney hyperelastic law (experiment shown with a dashed line, the model with a solid line).

Table 2
Materials parameters for the NR material.

Hyperelasticity			Internal sliding			
m_1	m_2	K	C_{20}	C_x	σ_s	γ
0.12 MPa	0.5 MPa	500	0.06 MPa	1.5 MPa	0.21 MPa	0.6

Table 3
Materials parameters for the SBR material (Mooney law).

Hyperelasticity			Internal sliding			
m_1	m_2	K	C_{20}	C_x	σ_s	γ
0.6 MPa	0.28 MPa	500	0.26 MPa	1.2 MPa	0.9 MPa	5

Table 4
Materials parameters for the filled SBR material (Hart-Smith law).

Hyperelasticity				Internal sliding			
h_1	h_2	h_3	K	C_{20}	C_x	σ_s	γ
1.6 MPa	0.28 MPa	5.29×10^{-4}	2000	0.14 MPa	0.93 MPa	1.16 MPa	0.57

mm) are given in Fig. 13 together with loading conditions. Due to symmetries, only one quarter of the specimen was simulated. A perfect adhesion between rubber and metal (steel) is assumed. The structure is meshed using 3D 20-nodes bricks using reduced integration (8 G points). The metal parts are assumed elastic (Young modulus E = 200 GPa and Poisson ratio $\nu = 0.3$). The material parameters for rubber are those obtained from the uniaxial test of filled rubber in Section 5 (see Table 2). Simulation was carried out using a mixed displacement–pressure finite element formulation using Penn-invariants. Using a standard displacement based formulation leads to a very similar global behavior. Fig. 14 shows the comparison between the experiment and the simulation. The description of hysteresis and cyclic softening reaches then same agreement with experiments than the one obtained for the test used to fit the material parameters, but this time in case of a 3D representative structure.

The deformed meshes are given in Fig. 15 with maps of π variable. The feature of a monotonic increase of π even during unloading illustrates the fact that π can be considered as a cumulative measure of the internal sliding.

7. Conclusions

The large strain cyclic mechanical behavior of elastomers has been investigated in this paper. A 3D constitutive model of internal sliding and friction (ISF model) accounting for hysteresis and cyclic stress softening has been presented. Stress softening is interpreted as being caused by sliding between polymeric chains and fillers and not by damage (i.e. microcracking or particle/matrix debonding). The constitutive model decomposes the material behavior into an hyperelastic part, a rate independent sliding part incorporating internal back stresses. The model has been calibrated against experiments carried out on filled natural rubber and filled styrene butadiene rubber. The model can be further developed introducing several internal slip variables corresponding to different slip mechanisms. This extension is straightforward but requires fitting additional material parameters. Accounting for viscosity has been already proposed in the paper; however, a model able to represent the different stress relaxation behaviors observed during loading and unloading still needs to be validated.

Acknowledgments

The authors gratefully acknowledge the experimental support of Paulstra–Hutchinson at Lisse France and particularly M. Pompei for many helpful discussions on the experimental aspects of this work.

Appendix A. Integration method for the constitutive equations

As presented in Section 4.1, the integration relies on an implicit mid-point strategy (see Eq. (21)). Auxiliary quantities $(\boldsymbol{n}, \boldsymbol{\alpha}, \boldsymbol{X})$ have to be computed at time $t^\theta = t^0 + \theta\Delta t$. These values, referred to as $(\boldsymbol{n}^\theta, \boldsymbol{\alpha}^\theta, \boldsymbol{X}^\theta)$, are calculated as follows:

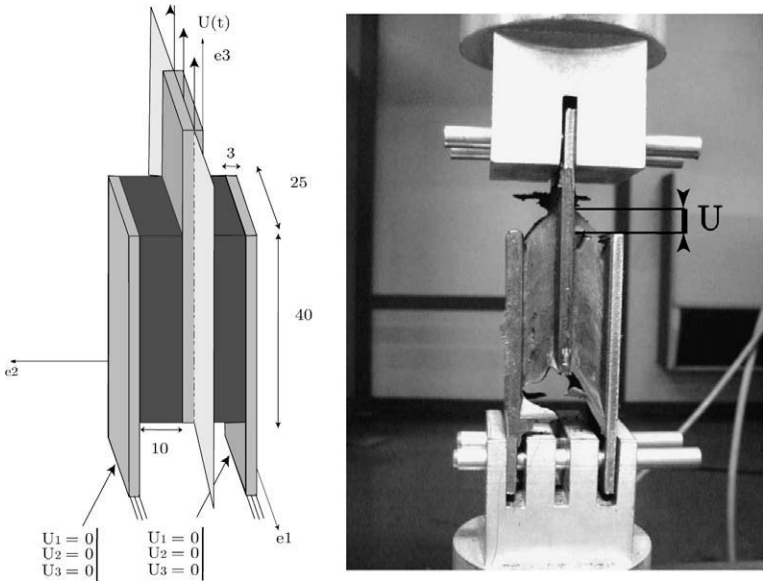

Fig. 13. Metal/elastomer lap joint (unit: mm).

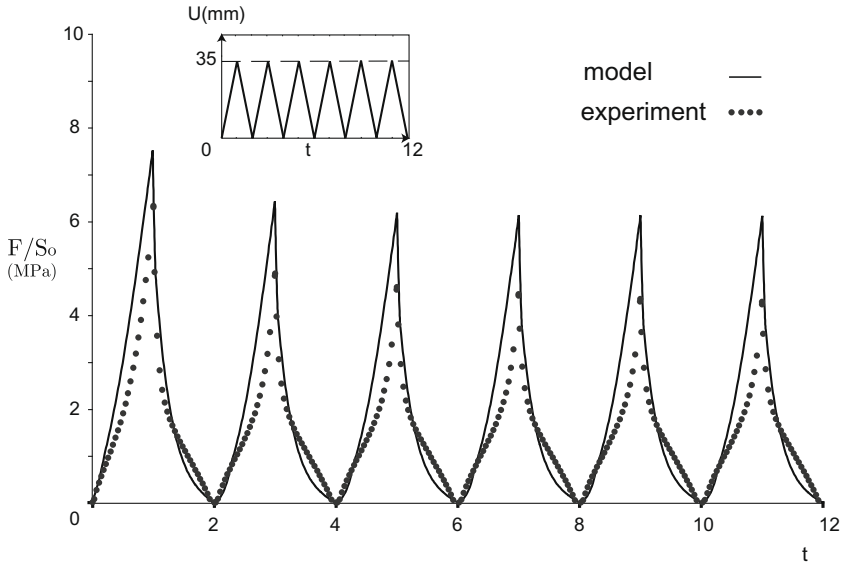

Fig. 14. Simulation of the metal/elastomer (NR) lap joint using material parameters given in Table 2.

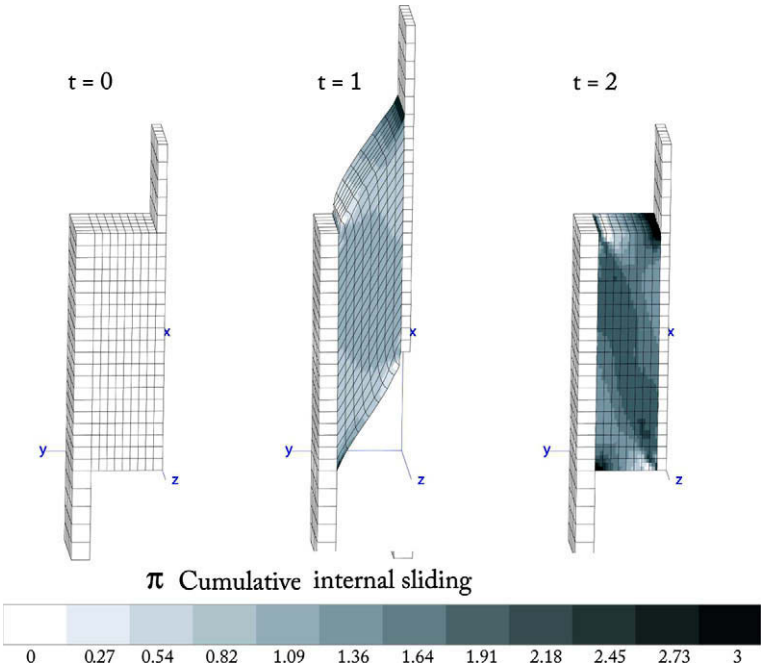

Fig. 15. Mesh and maps of cumulative measure of the internal sliding π at times $t = 0, 1, 2$.

$$\boldsymbol{\alpha}^{\theta} = \boldsymbol{\alpha}^{0} + \theta\Delta\boldsymbol{\alpha}, \quad \boldsymbol{E}^{\pi\theta} = \boldsymbol{E}^{\pi 0} + \theta\Delta\boldsymbol{E}^{\pi}, \quad \boldsymbol{E}^{\theta} = \boldsymbol{E}^{0} + \theta\Delta\boldsymbol{E},$$
$$\boldsymbol{X}^{\theta} = C_x\boldsymbol{\alpha}^{\theta}, \quad \boldsymbol{S}_2^{\theta} = 8C_{20}\mathrm{tr}(\boldsymbol{E}^{\theta} - \boldsymbol{E}^{\pi\theta})\mathbf{1}, \quad \boldsymbol{n}^{\theta} = \frac{\boldsymbol{S}_2^{\theta} - \boldsymbol{X}^{\theta}}{\|\boldsymbol{S}_2^{\theta} - \boldsymbol{X}^{\theta}\|}. \tag{A.1}$$

The superscript 0 indicates the known values at t^0. It is interesting to note that using an implicit integration scheme allows to avoid using the consistency condition which can be complex to write (Besson et al., 2001). The consistency condition is then replaced by expressing that the integrated solution must meet the yield condition, $f^{\theta} = 0$. This condition can be expressed at time t^{θ} but as it is preferable to meet the condition at the end of the increment. The yield condition is expressed at t^1 using the corresponding values of $\boldsymbol{S}_2$ and $\boldsymbol{X}$ (i.e. the second form of Eq. (22) which uses $\boldsymbol{S}_2^1$ and $\boldsymbol{X}^1$ calculated using Eq. (A.1) with $\theta = 1$). This solution is used in the following.

At this point, integrating the constitutive equations is equivalent to solve the system of the nonlinear equation (22). The system can be rewritten introducing a residual vector $\mathbf{R} = (\boldsymbol{R}_{\pi}, \boldsymbol{R}_{\alpha}, R_{\mu})$:

$$\begin{aligned} \boldsymbol{R}_{\pi} &= \Delta\boldsymbol{E}^{\pi} - \Delta\mu\,\boldsymbol{n}^{\theta}, \\ \boldsymbol{R}_{\alpha} &= \Delta\boldsymbol{\alpha} - \Delta\boldsymbol{E}^{\pi} + \gamma\Delta\mu\,\boldsymbol{\alpha}^{\theta}, \\ R_{\mu} &= \|\boldsymbol{S}_2^1 - \boldsymbol{X}^1\| - \sigma_s. \end{aligned} \tag{A.2}$$

The solution $\mathbf{R} = \mathbf{0}$ is searched with respect to the increment of the variables considered as unknowns $\Delta\mathscr{V} = (\Delta\boldsymbol{E}^{\pi}, \Delta\boldsymbol{\alpha}, \Delta\mu)$ using an iter-

ative Newton–Raphson method. The Jacobian, **J**, of the system (Eq. (A.2)) is therefore required. It can be computed as a block matrix as:

$$\mathbf{J} = \frac{\partial \mathbf{R}}{\partial \Delta \mathscr{V}} = \begin{pmatrix} \frac{\partial \boldsymbol{R}_\pi}{\partial \Delta \boldsymbol{E}^\pi} & \frac{\partial \boldsymbol{R}_\pi}{\partial \Delta \boldsymbol{\alpha}} & \frac{\partial \boldsymbol{R}_\pi}{\partial \Delta \mu} \\ \frac{\partial \boldsymbol{R}_\alpha}{\partial \Delta \boldsymbol{E}^\pi} & \frac{\partial \boldsymbol{R}_\alpha}{\partial \Delta \boldsymbol{\alpha}} & \frac{\partial \boldsymbol{R}_\alpha}{\partial \Delta \mu} \\ \frac{\partial R_\mu}{\partial \Delta \boldsymbol{E}^\pi} & \frac{\partial R_\mu}{\partial \Delta \boldsymbol{\alpha}} & \frac{\partial R_\mu}{\partial \Delta \mu} \end{pmatrix} \tag{A.3}$$

The sub-matrices are:

$$\frac{\partial \boldsymbol{R}_\pi}{\partial \Delta \boldsymbol{E}^\pi} = \underline{\mathbf{1}} + \frac{8C_{20}\theta\Delta\mu}{\left\|\boldsymbol{S}_2^\theta - \boldsymbol{X}^\theta\right\|}(\mathbf{1}\otimes\mathbf{1} - \mathrm{tr}(\boldsymbol{n})(\boldsymbol{n}\otimes\mathbf{1})) \tag{A.4}$$

$$\frac{\partial \boldsymbol{R}_\pi}{\partial \Delta \boldsymbol{\alpha}} = \frac{C_x\theta\Delta\mu}{\left\|\boldsymbol{S}_2^\theta - \boldsymbol{X}^\theta\right\|}\left(\underline{\mathbf{1}} - \boldsymbol{n}^\theta \otimes \boldsymbol{n}^\theta\right) \tag{A.5}$$

$$\frac{\partial \boldsymbol{R}_\pi}{\partial \Delta \mu} = -\boldsymbol{n}^\theta \tag{A.6}$$

$$\frac{\partial \boldsymbol{R}_\alpha}{\partial \Delta \boldsymbol{E}^\pi} = -\underline{\mathbf{1}} \tag{A.7}$$

$$\frac{\partial \boldsymbol{R}_\alpha}{\partial \Delta \boldsymbol{\alpha}} = (1+\gamma\theta\Delta\mu)\underline{\mathbf{1}} \tag{A.8}$$

$$\frac{\partial \boldsymbol{R}_\alpha}{\partial \Delta \mu} = \gamma\boldsymbol{\alpha}^\theta \tag{A.9}$$

$$\frac{\partial R_\mu}{\partial \Delta \boldsymbol{E}^\pi} = -8C_{20}\mathrm{tr}(\boldsymbol{n}^1)\mathbf{1} \tag{A.10}$$

$$\frac{\partial R_\mu}{\partial \Delta \boldsymbol{\alpha}} = -C_x\boldsymbol{n}^1 \tag{A.11}$$

$$\frac{\partial R_\mu}{\partial \Delta \mu} = 0 \tag{A.12}$$

Once convergence of the iterative process is reached, the stress tensor at the end of the increment can be computed as $\boldsymbol{S} = \boldsymbol{S}_1^1 + \boldsymbol{S}_2^1$ using the state law (3).

References

Armstrong, P.J., Frederick, C.O.,1966. A mathematical representation of the multiaxial Bauschinger effect. CEBG R.D./B/N731. Central Electricity Generating Board.

Andrieux, F., Saanouni, K., Sidoroff, F., 1997. Sur les solides hyperélastiques à compressibilité induite par l'endommagement. C.R. Acad. Sci. Paris Ser. IIb 324, 281–288.

Arruda, E.M., Boyce, M.C., 1993. A three-dimensional constitutive model for the large stretch behavior of rubber elastic materials. J. Mech. Phys. Solids 41, 389–412.

Beatty, M.F., Krishnaswamy, S., 2000. Theory of stress-softening in incompressible isotropic materials. J. Mech. Phys. Solids 48 (9), 1931–1965.

Besson, J., Cailletaud, G., Chaboche, J.L., Forest, S., 2001. Mécanique des matériaux solides. Hermes Sci..

Bueche, F., 1960. Molecular basis for Mullins effect. J. Appl. Polym. Sci. 4 (10), 107–114.

Burr, A., Hild, F., Leckie, F.A., 1997. Continuum description of damage in ceramic–matrix composites. Eur. J. Mech. A 16 (1), 53–78.

Cantournet, S., 2002. Endommagement et fatigue des élastomères, Ph.D. Thesis, Univ. Paris VI.

Dannenberg, E.M., 1975. The effet of surface chemical interactions on the properties of filler-reinforced rubbers. Rubber Chem. Technol. 44, 440–478.

Doll, S., Schweizerhof, K., 2000. On the development of volumetric strain energy functions. J. Appl. Mech. Trans. ASME 67, 17–21.

Dragon, A., Halm, D., 1998. An anisotropic model of damage and frictional sliding for brittle materials. Eur. J. Mech. A 17 (3), 439–460.

Flory, P.J., 1961. Thermodynamic relations for high elastic materials. Trans. Faraday Soc. 57, 829–838.

Godvindjee, S., Simo, J., 1991. A micro-mechanically based continuum damage model for carbon black-filled rubbers incorporating Mullins effect. J. Mech. Phys. Solids 29 (1), 87–112.

Halphen, B., 1975. Sur les matériaux standards généralisés. J. Mecanique 14, 39–63.

Harwood, J.A.C., Payne, A.R., 1966. Stress-softening in natural rubber vulcanizates. Part III: carbon black-filled vulcanizates. J. Appl. Polym. Sci. 10, 315–324.

Harwood, J.A.C., Payne, A.R., 1968. Hysteresis and strength of rubbers. J. Appl. Polym. Sci. 12, 889–901.

Holzapfel, G.A., 2001. Nonlinear Solid Mechanics: A Continuum Approach for Engineering, second ed. Wiley, New York.

Hughes, T.J.R., 1980. Generalization of selective integration procedures to anisotropic and non-linear media. Int. J. Numer. Meth. Eng. 15, 1413–1418.

Johnson, M.A., Beatty, M.F., 1993. The Mullins effect in uniaxial extension and its influence on the transverse vibration of a rubber string. Continuum Mech. Thermodyn. 5, 83–115.

Lambert-Diani, J., Rey, C., 1999. New phenomenological behavior laws for rubbers and thermoplastic elastomers. Eur. J. Mech. A 18, 1027–1043.

Lapra, A., 1999. Caractérisation moléculaire et propriétés mécaniques des réseaux élastomères sbr renforcés par la silice, Ph.D. Thesis, Univ. Paris VI.

Lemaitre, J., Chaboche, J.L., 1985. Mécanique des matériaux solides. Dunod, Paris.

Lemaitre, J., Desmorat, R., 2005. Engineering Damage Mechanics: Ductile, Creep, Fatigue and Brittle Failures. Springer, Berlin.

Miehe, C., 1995. Discontinuous and continuous damage evolution in Ogden-type large-strain elastic materials. Eur. J. Mech. A 14 (5), 697–720.

Miehe, C., Keck, J., 2000. Superimposed finite elastic-viscoelastic–plastoelastic stress response with damage in filled rubbery polymers. Experiments, modelling and algorithmic implementation. J. Mech. Phys. Solids 48, 323–365.

Mullins, L., 1947. Effect of stretching on the properties of rubber. J. Rubber Res. 16, 275–289.

Mullins, L., Tobin, N.R., 1954. Theoretical model for the elastic behavior of filler-reinforced vulcanized rubbers. In: Proceedings of the Third Rubber Technological Conference, W. Heffer and Sons Ltd., pp. 397–412.

Mullins, L., Tobin, N.R., 1965. Stress softening in rubber vulcanizates. Part I. J. Appl. Polym. Sci. 9, 2993–3009.

Oden, J.T., 1972. Finite Elements of Nonlinear Continua. McGraw-Hill, New York.

Ogden, R.W., 1982. Elastic deformation of rubberlike solids, In: Mechanics of Solids, vol. 6, The Rodney Hill 60th Anniversary Volume, Pergamon Press, Oxford, pp. 499–537.

Ogden, R.W., roxburgh, D.G., 1999. A pseudo-elastic model for the Mullins effect in filled rubber. Proc. Roy. Soc. Lond. A 455, 2861–2877.

Penn, R.W., 1970. Volume changes accompanying the extension of rubber. Trans. Soc. Rheol. 14 (4), 509–517.

Qi, H.J., Boyce, M.C., 2004. Constitutive model for stretch-induced softening of the stress-stretch behavior of elastomeric materials. J. Mech. Phys. Solids 52 (10), 2187–2205.

Rivlin, R.S., 1948. Large elastic deformations of isotropic materials. Philos. Trans. Roy. Soc. Lond. A 240, 459–481.

Simo, J.C., 1987. On a fully three-dimensional finite-strain visco-elastic damage model: formulation and computational aspects. Comput. Meth. Appl. Mech. Eng. 60, 153–173.

Simo, J.C., Taylor, R.L., Pister, K.S., 1985. Variational and projection methods for the volume constraint in finite deformation elastoplasticity. Comput. Meth. Appl. Mech. Eng. 51, 177–208.

Taylor, R.L., 2000. A mixed-enhanced formulation for tetrahedral finite elements. Int. J. Numer. Meth. Eng. 47, 205–227.

Truesdell, C., Noll, W., 1965. The non-linear field theories of mechanics. Handbuch der Physik, III 3. Springer, Berlin.

Vidal, A., Donnet, J.B., 1986. Carbon black: surface properties and interactions with elastomers. Adv. Polym. Sci. 76, 104–106.

Zuniga, A.E., Beatty, M.F., 2002. A new phenomenological model for stress-softening in elastomers. Z. Angew. Math. Phys. 53 (5), 794–814.